Accelerating the Lagrangian particle tracking of residence time distributions and source water mixing towards large scales

Chen Yang[a], You-Kuan Zhang[b,c], Xiuyu Liang[b,c], Catherine Olschanowsky[d]

Xiaofan Yang[e]*, Reed Maxwell[a]*

[a]Department of Civil and Environmental Engineering and the Princeton Environmental Institute, Princeton University, Princeton, NJ 08544, USA. e-mail: reedmaxwell@princeton.edu

[b]Guangdong Provincial Key Laboratory of Soil and Groundwater Pollution Control, School of Environmental Science and Engineering, Southern University of Science and Technology, Shenzhen 518055, China.

[c]State Environmental Protection Key Laboratory of Integrated Surface Water-Groundwater Pollution Control, School of Environmental Science and Engineering, Southern University of Science and Technology, Shenzhen 518055, China.

[d]Computer science department, College of Engineering, Boise State University, Boise, ID 83704, USA.

[e]State Key Laboratory of Earth Surface Processes and Resource Ecology, Faculty of Geographical Science, Beijing Normal University, Beijing 100875, China. e-mail: xfyang@bnu.edu.cn

*Corresponding author

All codes for this work are publicly available on GitHub along with the Hillslope model used for the simulations: https://github.com/reedmaxwell/EcoSLIM

This manuscript has been submitted for publication in *Computers & Geosciences*. Please note that, despite having undergone peer-review, the manuscript has yet to be formally accepted for publication. Subsequent versions of this manuscript may have slightly different content. If accepted, the final version of this manuscript will be available via the 'Peer-reviewed Publication DOI' link on the right-hand side of this webpage. Please feel free to contact any of the authors; we welcome feedback.

Dr. Chen Yang was responsible for code development, code tests, and manuscript preparation. Dr. Zhang and Liang assisted with the computing resources. Dr. Olschanowsky assisted with the code development. Dr. Xiaofan Yang assisted with the code development, computing resources, and manuscript preparation. Dr. Maxwell assisted with the code development, code tests, and manuscript preparation.

Abstract

Travel/residence time distributions (TTDs/RTDs) are important tools to evaluate the vulnerability of catchments to contamination and understand many aspects of catchment function and behavior. In recent years, the calculation of TTDs/RTDs based on the Lagrangian particle tracking approach together with the integrated hydrologic modeling has become a popular counterpart to analytical approaches and lumped numerical models. As global water availability becomes more stressed due to anthropogenic disturbance and climate change, the requirement of large-scale and long-term simulations for TTDs/RTDs further pushes the high computational costs of Lagrangian particle tracking. Hence, speeding up the Lagrangian particle tracking approach becomes an important barrier to advancement. In this study, we accelerate the Lagrangian particle tracking program EcoSLIM, using a combination of distributed (e.g. MPI) and multi-core accelerator (CUDA) approaches for large-scale and long-term simulations. EcoSLIM was developed to be seamlessly paired with the integrated ParFlow.CLM model for calculations of transient RTDs and source water mixing and was originally developed using threaded OpenMP. This work extends this implementation to compare combinations of MPI, CUDA and OpenMP. Of these combinations, the OpenMP-CUDA parallelism performed the best moving from single-GPU to multi-GPU. The multi-GPU shows strong scalability which becomes increasingly efficient with more particles, demonstrating a potential feasibility for regional-scale, transient residence time simulations. This work largely improves the computational capability of EcoSLIM, and results also show the advantages of using GPU-parallel to traditional parallel-APIs (application programming interfaces) and its potential to widely accelerate the next generation programs in subsurface environment modeling.

Keywords: Lagrangian particle tracking, Integrated modeling, Travel/residence time distributions, MPI, Multi-GPU

1. Introduction

Travel time distribution (TTD) and residence time distribution (RTD) are probability density functions of age for water parcels leaving from and storing in the catchment subsurface (Yang *et al.*, 2018). Both TTD and RTD are important tools to reflect how catchments retain and release water which in turn indicate the storage and turnover of the contaminants (Jing *et al.*, 2019; Kirchner *et al.*, 2000; McDonnell *et al.*, 2010; van der Velde *et al.*, 2010; Yang *et al.*, 2018). Traditionally, analytical approaches and lumped numerical models are common tools to determine the TTDs/RTDs (Basu *et al.*, 2012; Benettin *et al.*, 2015; Benettin *et al.*, 2013a; Benettin *et al.*, 2013b; Botter *et al.*, 2011; Engdahl *et al.*, 2016; Kirchner *et al.*, 2001; Małoszewski and Zuber, 1982; McDonnell *et al.*, 2010).

However, in recent years, Lagrangian particle tracking together with physically-based, integrated hydrological models has emerged as a promising tool for estimating TTD/RTD (Danesh-Yazdi *et al.*, 2018; de Rooij *et al.*, 2013; Engdahl and Maxwell, 2015; Engdahl *et al.*, 2016; Jing *et al.*, 2019; Jing *et al.*, 2020; Wilusz *et al.*, 2019; Yang *et al.*, 2018). Though particle tracking generally is more computationally efficient than most Eulerian approaches (Tompson and Gelhar, 1990; Yang *et al.*, 2018), the computation burden can still be quite high if fine spatial and temporal resolutions or large-scale and long-term simulations are considered. As such, most of the current studies are limited by the total number of particles thus constraining the problem size or simulation duration. For example, the study areas of some recent applications, e.g. Yang *et al.* (2018), Weill *et al.* (2019), and Wilusz *et al.* (2019) are quite small, only 1.44-, 0.8-, and 0.4-km^2 respectively. Wilusz *et al.* (2019) adopted an hourly timestep while the total simulation time was 3 years. Though a longer, 10-year simulation was conducted by Yang *et al.* (2018), a daily timestep was used. Similar studies with larger scale study area but coarse timestep include but not limited

to the Nägelstedt catchment of 850 km^2 in Jing *et al.* (2019) and Jing *et al.* (2020) and the Little Washita watershed of about 600 km^2 in Kollet and Maxwell (2008b). While the continental US of 6.3×10^6 km^2 was simulated in Maxwell *et al.* (2016), this simulation was steady-state, and the particles were run separately in several subsets of the domain.

More importantly, the objectives of these large-scale studies are all TTDs of outflow (streamflow) instead of RTDs of groundwater. Simulation of TTDs is conducted by injecting a fixed number of particles and tracking them until all of them leave the modeling domain. Whereas, the simulation of RTDs has to be spun-up; running the system to a dynamic equilibrium when particles filling up the subsurface (Maxwell *et al.*, 2019; Yang *et al.*, 2018). The number of total particles required for RTDs cannot be determined *a priori*, which results in a much higher computational requirement for RTDs than TTDs. With the recent advances in TTDs/RTDs, the travel time of evapotranspiration (i.e., the evapotranspiration time) (Botter, 2012; Maxwell *et al.*, 2019) and the age of pumped groundwater under anthropogenic disturbance, have the same requirement of reaching a dynamic equilibrium. In addition, under the climate change, long-term simulations are necessary for in-depth understanding of the RTDs (Jing *et al.*, 2020; Manning *et al.*, 2012; Yang *et al.*, 2018). Last but not least, transport modeling at larger scales also motivates further development of Lagrangian particle tracking (Hartmann *et al.*, 2020; Jing *et al.*, 2019; LaBolle *et al.*, 1996; Tompson, 1993; Tompson and Gelhar, 1990). As a result, it is critical to accelerate the computation speed of the Lagrangian particle tracking.

Modeling platforms including both hardware and software are required to meet the increasing demand of memory and speed, which can benefit the continuous development of subsurface environmental modeling, and, otherwise, would be a bottleneck (Jacobsen *et al.*, 2010; Scheibe and Smith, 2015). CPUs (Central Processing Units)-based high performance clusters are generally

used to solve computationally expensive problems. MPI (Message Passing Interface)-based ParFlow.CLM (Kollet and Maxwell, 2008a), PFLOTRAN (Hammond *et al.*, 2014), ParMIN3P-THCm (Su *et al.*, 2017), and eSTOMP (Freedman *et al.*, 2016) are representatives in massively-parallel groundwater and/or reactive transport models (Steefel *et al.*, 2015). Particularly, Engdahl *et al.* (2019) parallelized the Lagrangian simulations of mixing-limited reactive transport using MPI based on a novel parallel particle scheme. OpenMP (Open Multi-Processing), supporting shared memory multi-threading programming on CPU, is also widely used, which, however, when used as the only parallelization strategy is more suitable for medium-size computation or on personal workstations. OpenMP can also be nested within MPI for further intra-node speedup on clusters. Typical examples are the current version of EcoSLIM (Maxwell *et al.*, 2019) using OpenMP and the TOUGHREACT using hybrid MPI-OpenMP (Steefel *et al.*, 2015).

Since 2005, the application of GPU (Graphics Processing Unit) to scientific computing has attracted more attention due to the large number of cores contained within each GPU. With the appearance of NVIDIA's CUDA (Compute Unified Device Architecture) in 2007, GPU-based parallel programing has been increasingly utilized in scientific computing (Ruetsch and Fatica, 2014). In geoscientific modeling, GPU-based acceleration mainly focus on earth system models such as the atmosphere and ocean models (Porter *et al.*, 2018; Xu *et al.*, 2015). MIKE 21 GPU is the GPU-parallel version of MIKE 21 which is for coastal modeling (DHI, 2019). GPUs have also been widely used in particle/lattice-based computational fluid dynamics (CFD) methods and simulations (Cheng *et al.*, 2015; Jacobsen *et al.*, 2010; Molinero *et al.*, 2019). Whereas, the GPU-parallelism is still in its infancy in modeling the subsurface environment and related integrated modeling. Ji and her collaborators conducted GPU-parallel on MODFLOW and MODPATH (Ji *et al.*, 2010; Ji *et al.*, 2014; Ji *et al.*, 2019; Sun *et al.*, 2019). The reported speedup of MODFLOW

115 using NVIDIA Tesla C1060 is 1.6- to 10.6-fold for models with more than 10^5 cells while the
116 speedup of MODPATH on simulating more than 5 million streamlines is over 1000 by using 8
117 NVIDIA GPUs. However, for the next generation code/program handling coupled processes at
118 large scales, the CUDA-version ParFlow is expected to become a powerful tool (Kuffour *et al.*,
119 2020).

120 EcoSLIM (Maxwell *et al.*, 2019), based on a Lagrangian particle tracking approach, works
121 seamlessly with ParFlow.CLM, an integrated hydrologic model (IHM) coupling the groundwater
122 model and land surface model (Kuffour *et al.*, 2020; Maxwell and Miller, 2005). The current
123 EcoSLIM focuses on transient RTDs of different hydrological components at the watershed scale,
124 such as groundwater in variably-saturated zone, evapotranspiration (ET), and outflow. The latter
125 two are the same to travel times of ET and outflow mentioned above. Another feature of EcoSLIM
126 is to identify the source water mixing of hydrological components (Maxwell *et al.*, 2019). For
127 example, ET particles that exit the modeling domain can be further characterized by source water
128 composition: for example, the fractions of groundwater, rain, or snow. Particularly, the RTD of
129 ET and the source water mixing are rarely addressed in previous modeling approaches (Maxwell
130 *et al.*, 2019), which makes EcoSLIM as a promising tool to model RTDs by IHM and particle
131 tracking, advancing the work of lumped models and more simple analytical solutions. Nested
132 within ParFlow.CLM, EcoSLIM also has a possible extension to large-scale contaminant transport
133 modeling, which can trace the sources and traveling trajectories of the contaminants as well as
134 calculate the RTDs that are important for remediation.

135 The objective of this study is to accelerate the EcoSLIM code for large-scale and long-term
136 simulations. The EcoSLIM code was extended to include MPI and GPU parallelism. This was
137 constructed using both the CPU-based MPI and the GPU-based CUDA Fortran as extensions to

its original OpenMP parallel formulation. More importantly, different approaches from single GPU to multi-GPU were inter-compared and evaluated. The rest of this article is organized as follows. In the second section, the parallelism currently in EcoSLIM (i.e., the particle loops) is identified and profiled; the implementation of new parallelism with different APIs (application programming interfaces) is described. In the third section, the model setup and hardware for a suite of test cases are introduced. Then the simulation results from MPI- and CUDA-parallel are verified against those from the original OpenMP-parallel, which are presented to demonstrate the accuracy of new parallel approaches. In the fourth section, the computation performance of three parallel-APIs are intercompared. The computation capability based on multi-GPU is compared to previous studies, which to the best of our best knowledge, is the first time. Finally, conclusions are drawn for this study.

2. Methodology

2.1. The parallel particle loop in EcoSLIM

We first evaluated the computational cost of EcoSLIM using the hillslope model introduced in Maxwell *et al.* (2019). Details of the hillslope model are presented later in section 3.1. Using one CPU thread based on OpenMP, results show that the time used by the particle loop in EcoSLIM is over 99.8% of the total simulation time (Table 1). Hence, the parallelization in this study is conducted only for the particle loop in EcoSLIM. A flow chart of the particle loop is shown in Fig. 1, with key variables summarized in Table 2. For each active particle in a global timestep (i.e., the timestep in ParFlow), the execution proceeds as follows:

a) It is first looped by the local particle timestep. This loop continues until the total accumulated time is larger than the current global timestep. Then the adjacent cell of this particle (#9) and the grid-cell aggregated information [$C(1{:}5, :, :, :)$] (#10) are updated.

b) In the local time loop, the adjacent cell of a particle is determined by its coordinates [*P*(:,1:3)] (#1). Next, cell fractions in x, y, and z directions of a particle are determined (#3) before its advection velocities being linearly interpolated from the velocities (variables 12–14 in Table 2) distributed on cell-interfaces (#4). Thus, the local particle timestep can be calculated (#5).

c) The location of the particle is updated together with the deviation caused by molecular diffusion (#7). Finally, the particle's trajectory is amended with the reflection principle (LaBolle et al., 1996) if the particle is out of the domain (#8).

d) In the local time loop of each particle, whether the particle is out of the domain either through outflow or ET is evaluated (#2 and #6). If a particle leaves as outflow or ET, its status is switched to inactive. Meanwhile, the age, mass, composition, and particle-number of the outflow or ET are updated (variables 3–10 in Table 2). For ET, *C* array [*C*(6:9, :, :, :)] is also updated for grid-cell aggregated information of ET.

Table 1. Baseline simulation time for EcoSLIM using one CPU thread based on OpenMP

Case name	Particle loop (hour)	Total time (hour)	Percentage (Loop/Total)
ER_Shrubs	33.81	33.87	99.83%
ER_Trees	70.21	70.33	99.83%
LW_Shrubs	111.02	111.21	99.83%
LW_Trees	84.54	84.70	99.81%

Table 2. Key variables in the particle loop

Index	Array	Function	GPU memory
1	P(1:np,1:10)	np is the maximum permitted number of particles in the simulation. For each particle, from 1 to 10, the array includes: xyz coordinates, residence time (RT), saturated RT, mass, source, active/inactive status, concentration, and exit status.	Global/Shared. Copied to shared memory before computation and copied back to global memory after computation.
2	C(9,nx,ny,nz)	nx, ny, and nz are the grid dimension of the modeling domain. 1 to 9 is the grid-cell aggregated information: concentration, age, mass, source, P(:,9), ET particles, ET mass, ET age, and ET source.	Global. Atomic operations.
3	ET_age(pfnt,5)	pfnt is the total timesteps in the simulation. ET_age(:,1) is the mass weighted age of ET.	Global/Register

4	ET_comp(pfnt,3)	ET_comp(:,1:3) is the source water composition of ET mass. From 1 to 3: initial water, rain, and snowmelt.	Global/Register
5	ET_mass(pfnt)	The mass of ET.	Global/Register
6	ET_np(pfnt)	The number of particles exit as ET.	Global/Register
7	Out_age(pfnt,5)	The mass weighted age of outflow.	Global/Register
8	Out_comp(pfnt,3)	Out_comp(:,1:3) is the source water composition of outflow. From 1 to 3: initial water, rain, and snowmelt.	Global/Register
9	Out_mass(pfnt,5)	Out_mass(:,1) is the mass of outflow.	Global/Register
10	Out_np(pfnt)	Number of particles exit as outflow.	Global/Register. Variables 3–10 have private copies on registers. Atomic summation of threads on global memory is conducted.
11	dz(nz)	Vertical thickness of layers	Texture
12	Vx(nx+1,ny,nz)	Transient velocity in x direction.	Texture
13	Vy(nx,ny+1,nz)	Transient velocity in y direction.	Texture
14	Vz(nx,ny,nz+1)	Transient velocity in z direction.	Texture
15	Saturation(nx,ny,nz)	Saturation.	Texture
16	Porosity(nx,ny,nz)	Porosity.	Texture
17	EvapTrans(nx,ny,nz)	Evapotranspiration (ET). 12–15 and 17 change for each global timestep. Porosity keep constant in the whole simulation.	Texture

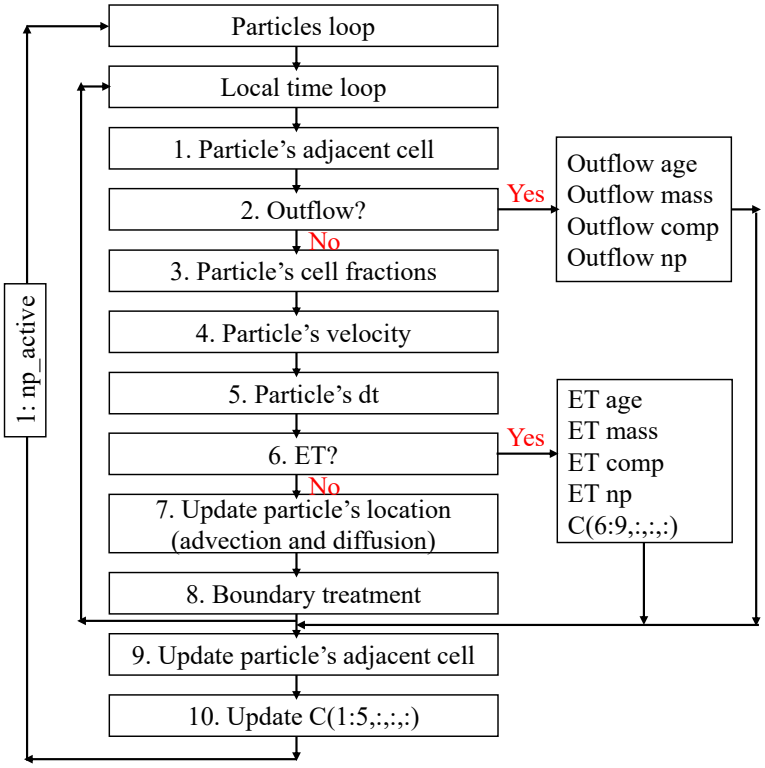

Fig. 1. Flow chart of the particle loop in a global timestep in EcoSLIM.

2.2. Memory management via CUDA-capable GPU

Memory management via CUDA-capable GPU is shown in Fig. 2. The shared memory, L1 cache, local memory, and registers are on-chip memory; while global, constant, and texture memories are all in DRAM (dynamic random-access memory) of the GPU device. There are also on-chip caches for constant and texture memories. Global memory can be read and written by both CPU and GPU, and it is available by all threads launched on GPU. Constant and texture memories can be read and written by CPU while they are read-only for threads on GPU. For each thread block, shared memory can be read and written by all threads in that block. Shared memory and L1 cache are configurable memories of 64 KB in total. Variables stored in registers are private for each thread. If the memory of registers is insufficient, data will be stored in local memory which is also thread private. CUDA Fortran, which was first developed in late 2009, is adopted for GPU programming in this study. CUDA Fortran can be implemented using The Portland Group® (PGI®) Fortran compiler which has the NVIDIA's CUDA architecture.

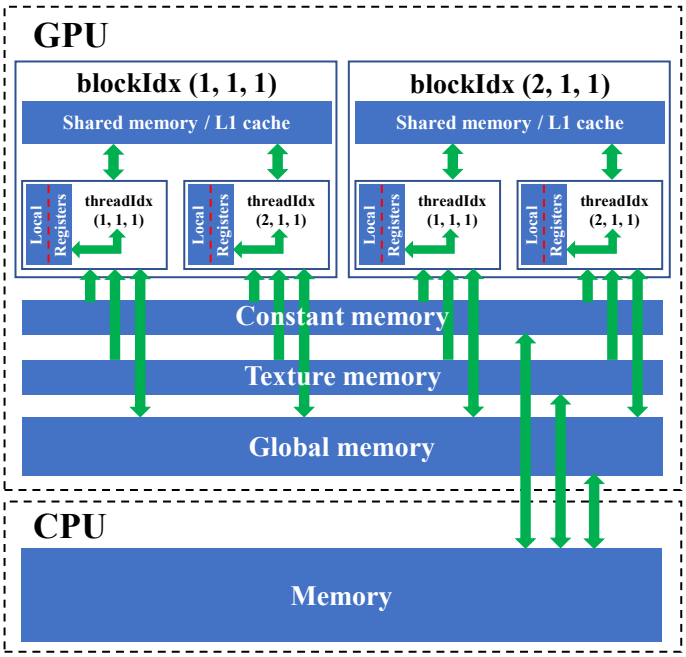

Fig. 2. Schematic of memory types on CUDA-capable GPU.

2.3. Parallel programing

2.3.1. OpenMP

The original EcoSLIM (Maxwell *et al.*, 2019) code was implemented in OpenMP and is described briefly here for comparison among different parallel APIs. The total *np_active* particles are implicitly decomposed by OpenMP and assigned to *n* threads (Fig. 3a). Threads number *n* can be set by the environment variable *OMP_NUM_THREADS* before starting the run. All variables in Table 2 and other public information (e.g., *np_active,* dimensions of modeling domain, global timestep) are shared by all threads while the particle-dependent information (e.g., particle's adjacent cell and cell fractions, random numbers for ET and diffusion, particle's velocities, etc.) are thread private. For calculations related to outflow, ET, and *C* in the particle loop (#2, #6, and #10 in Fig. 1), atomic operations are used to avoid the concurrent writing of these arrays by more than one thread.

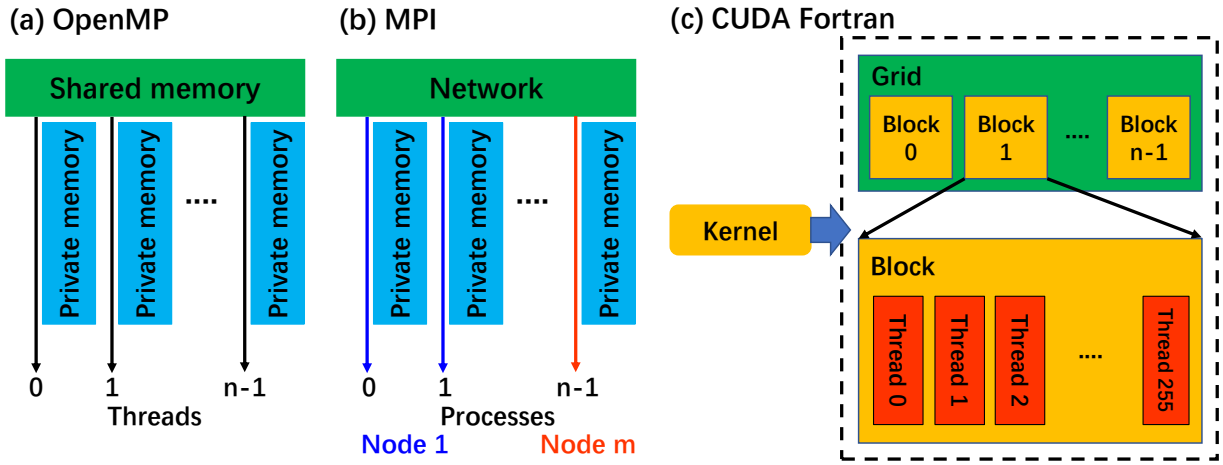

Fig. 3. Schematic of parallel programming using (a) OpenMP, (b) MPI, and (c) CUDA Fortran.

2.3.2. MPI

In each global timestep, the loop of *np_active* particles are evenly decomposed to *n* sub-loops. *n* is the number of processes launched in the run (Fig. 3b). Hence, *P*(1:*np_active*,:) is divided into

214 *n* segments. If *np_active* is not divisible by *n*, the remainder *m* particles are distributed to the first
215 *m* processes. *P* segments, velocities, saturation, ET, and porosity are then distributed from the root
216 process to others. New variables corresponding to variables 2–10 are declared and set as zero in
217 each global timestep before the sub-loop to gather the information of outflow, ET, and *C* on each
218 process. Once finished, the *P* array on the root process is updated by segments from other MPI
219 processes. ET, outflow, and *C* from each process represented by new variables are summed to
220 update variables 2–10 in Table 2.

221 **2.3.3. CUDA Fortran**

222 When implementing EcoSLIM on the GPU, one kernel is defined (Fig. 3c) and launched once
223 in each global timestep. Size of the thread block (*block_size*) is 256, and the number of thread
224 blocks is determined by *ceiling(real(np_active)/block_size)*. Taking the 1080 Ti GPU card as an
225 example, the maximum number of thread blocks permitted is 2,147,483,647; which is
226 549,755,813,632 threads in total if the block size is 256. This number is beyond the number of
227 particles in all test cases in this study, so each thread is responsible for only one particle.

228 Arrays of *P*, *C*, and ET and outflow (variables 1–10 in Table 2) are both read and written in
229 the particle loop and thus stored in the global memory. Input variables such as layer thickness,
230 porosity, velocities, saturation, and ET for each global timestep (variables 11–17 in Table 2) use
231 the read-only texture memory. Texture memory has caches on chip and can be accessed more
232 rapidly compared to global memory. It is also advantageous for noncontiguous access to these
233 arrays by threads because variables 12–17 in Table 2 are stored with the sequence by index of grid-
234 cells while threads are indexed by the sequence of particles in *P*. After *P* is copied from CPU to
235 GPU, it is further copied from global memory to shared memory of each thread block to improve
236 the efficiency of thread access.

237 In the GPU kernel, a group of thread-private variables for outflow and ET are declared using
238 registers. Outflow and ET information are first obtained on each thread without waiting. After the
239 particle loop, the summation of these variables (variables 3–10 in Table 2) on each thread are
240 computed by the reduction method used in the π computation with Monte Carlo method (Ruetsch
241 and Fatica, 2014). For the *C* array, atomic operation is directly performed in the particle loop. For
242 molecular diffusion and ET processes, random numbers are generated by a GPU function called
243 in the kernel function. After the execution, arrays of *P*, *C*, and ET and outflow (variables 1–10 in
244 Table 1) are copied back to CPU to update the information.

245 **2.3.4. Multi-GPU**

246 Three multi-GPU approaches were considered for EcoSLIM (Fig. 4): (1) Multi-GPU via
247 asynchronous data transfer with CUDA stream, (2) Multi-GPU with MPI, and (3) Multi-GPU with
248 OpenMP. For CUDA stream (Fig. 4a), the particle loop is equally divided into sub-loops, and each
249 GPU is assigned to one sub-loop. The total number of sub-loops is determined by the total number
250 of GPUs. Computation of sub-loops on GPUs use the same kernel explained in section 2.3.3. A
251 single CPU thread is used while the switch between different GPUs is through asynchronous data
252 transfers with specific CUDA stream for each GPU. Communication with MPI (Fig. 4b)/OpenMP
253 (Fig. 4c) is similar to that with CUDA stream (Fig. 4a), only that different GPUs are assigned to
254 different CPU processes/threads. The main difference between MPI and OpenMP is that processes
255 can belong to different computation nodes while all threads belong to the same node (Fig. 3a and
256 3b).

257 Obviously, for all three approaches using multi-GPU, the overhead on CPU is necessary to
258 decompose the loop of particles to sub-loops, distribute necessary information to different
259 streams/processes/threads, and combine results from different streams/processes/threads for

updates. For CUDA stream, this is realized by *do loops* while for MPI, this is realized by MPI communicators. However, for OpenMP, variables are simply set with shared or private attributes at the beginning of the parallel region. Through tests in this study, this overhead for CUDA stream and MPI is over the GPU time decreased by multi-GPU relative to the single GPU code in section 2.3.3. Therefore, CUDA stream and MPI are not suitable to parallelize EcoSLIM with current structure using multi-GPU and hence will not be discussed any more.

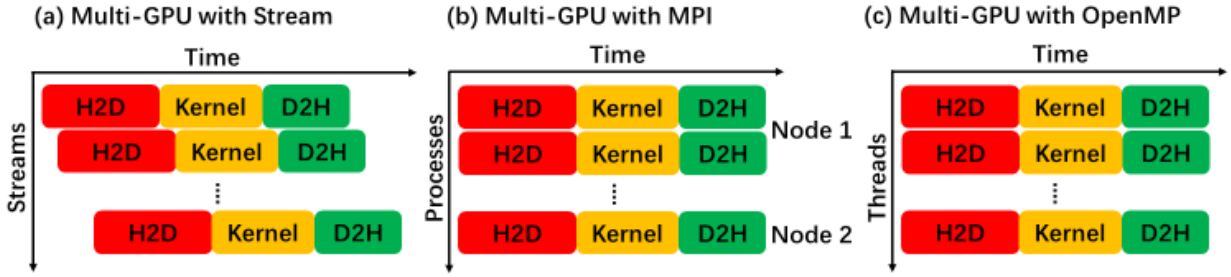

Fig. 4. Schematic of parallel programming using multi-GPU. H2D represents data transfer from CPU to GPU while D2H represents GPU to CPU.

3. Model setup, hardware, and validity of parallels

3.1. Hillslope model

The Hillslope model (Maxwell *et al.*, 2019) was adopted to test the parallel performance of EcoSLIM. Geometry of the modeling domain has the length of 100-, 1-, and 9.4-m in x, y, and z directions, respectively. It was divided into 20 columns, 5 rows, and 20 layers with constant resolutions of 5- and 0.2-m in x and y directions while, in z direction upward, various thickness of layers was set as: 0.5 m for the bottom 18 layers and 0.3- and 0.1-m for the top 2 layers. The soil properties are homogeneous, including saturated hydraulic conductivity of 0.05 m/h, Manning's N of 10^{-6} $m^{1/3}h^{-1}$, porosity of 0.2, and van Genuchten parameters with α of 1.0 m^{-1} and exponent n of 2.0. Two real meteorological-forcings were considered to drive ParFlow.CLM, representing a high elevation, snow dominated mountain headwaters (ER) and a semiarid, rain-dominated plains

system (LW). Two homogeneous land-cover types were used which are the Evergreen Needleleaf plant functional type (Trees) and the Shrub plant functional type (Shrubs). Thus, four cases were tested with combination of the meteorological forcings and the land-cover types named as: ER-Shrubs, ER-Trees, LW-Shrubs, and LW-Trees.

For both ParFlow.CLM and EcoSLIM, no flux boundaries were used except the top boundary which is open for precipitation and exit of outflow and ET. ParFlow.CLM simulations of 5 consecutive years with hourly timestep were conducted. One-year forcing data were repeatedly used in all the simulations. Dynamic equilibrium of the flow field was achieved at the end of the simulation for all four cases. Thus, the transient flow field in the last year of the 5-year simulation is repeatedly used in the EcoSLIM simulation of 20 years with hourly timestep. At the end of the simulation, EcoSLIM system achieved the dynamic equilibrium. By injecting 2 particles into the modeling domain per precipitation event, the mean particle-numbers in the last year of the simulation for four cases are 0.39, 0.83, 1.30, and 1.03 million, respectively. For the test in section 4.3, it was increased to 2000 particles per precipitation event to test the capability using multi-GPU toward large scales.

3.2. Hardware

The following platforms were used to test the OpenMP-, MPI-, and CUDA-version EcoSLIM. Platform (1) is to test OpenMP and MPI while (1), (2), and (3) are set for CUDA.

(1) A workstation. It is equipped with GeForce GTX 1080 Ti (GPU) and Intel® Xeon® CPU E5-2683 v3 @ 2.00GHz. There are 28 physical CPU cores with hyper-threading technology. The maximum available threads for OpenMP is 56 while the maximum available processes for MPI is 28 with the PGI compiler. The driver version for NVIDIA GPU is 440.33.01, CUDA version is 10.2, and PGI version is 19.10 with Open MPI of 3.1.3. All OpenMP, MPI, and CUDA version codes were compiled and built by the PGI compiler.

Tianhe-2 (TH-2) supercomputer in the National Supercomputer Center in Guangzhou, China, *gpu_v100 partition*. It has 4 GPU cards of Tesla V100 (SXM2, 16GB) per computation node and the CPU processor of Intel® Xeon® Gold 6132 CPU @ 2.60GHz. Driver version for NVIDIA GPU is 418.67, CUDA version is 10.1, and PGI version is 19.10.

(2) Tianhe-2 (TH-2) supercomputer in the National Supercomputer Center in Guangzhou, China, gpu partition. It has the GPU card of Tesla K80 (11 GB) and the CPU processor of Intel® Xeon® CPU E5-2660 v3 @ 2.60GHz. Driver version for NVIDIA GPU is 390.30, CUDA version is 8.0, and PGI version is 17.1.

3.3. Code-to-code verification: MPI- and CUDA-parallel of EcoSLIM

Taking outflow as an example, daily flow rate and residence time for four cases via MPI- and OMP were plotted in Fig. 5; while those using CUDA- and OMP were plotted in Fig. 6. OpenMP is abbreviated as OMP here. Only results for the last year of the 20-year simulation are shown due to the achievement of dynamic equilibrium in all simulations as mentioned in section 3.1. Results from MPI and CUDA are highly consistent with those from OMP for all cases, which demonstrated the accuracy of the parallel implementation. The little discrepancy between MPI/CUDA and OMP should be attributed to the generation of random numbers for initial position of particles, particles captured as ET, and random walk induced by molecular diffusion.

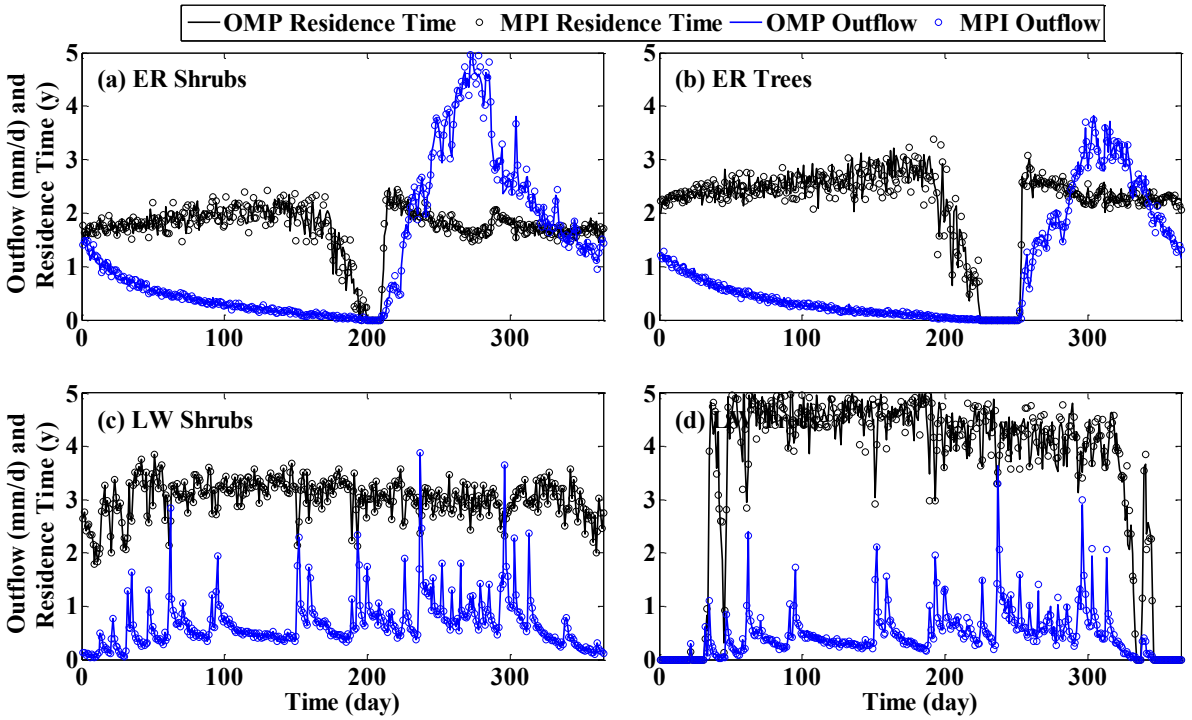

322
323 **Fig. 5. Comparison of residence time of outflow between MPI- and OMP-EcoSLIM**

324

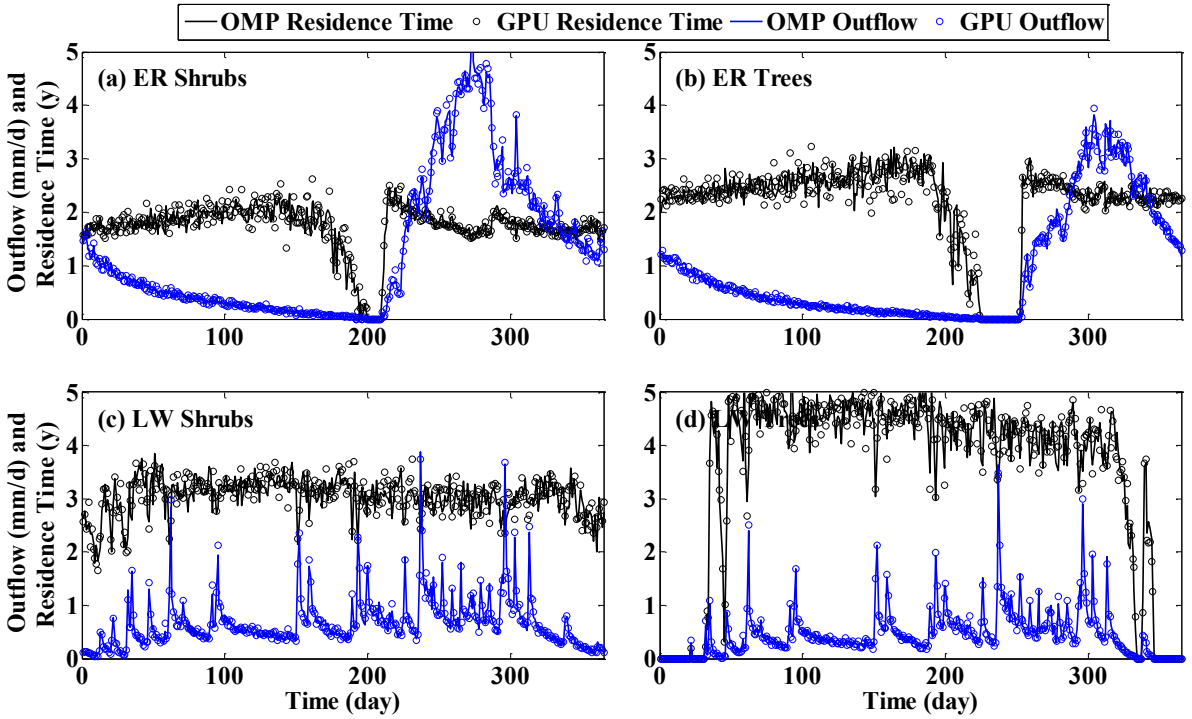

325
326 **Fig. 6. Comparison of residence time of outflow between CUDA- and OMP-EcoSLIM**

327

4. Parallel performance

4.1. Speedup by OMP and MPI

Scaling tests for OMP and MPI conducted on the workstation based on ER_Shrubs are shown in Fig. 7. For MPI using PGI compiler, a maximum of 28 processes can be launched since there are 28 CPU cores on the workstation. In general, MPI has the advantage that more processes can be used on the distributed architecture while the speedup by OMP may be limited by the number of CPU cores on one computational node. However, through the results from the scaling tests shown in Fig. 7, both OMP and MPI cannot unlimitedly speedup the computation with high efficiency even though CPU threads/processes are continuously increasing. For OMP, the time consumption decreases with increasing number of CPU threads to a maximum of 25 (3.74 h). The time used for 30 threads (3.78 h) is even more than that with 25 threads. Limited speedup can also be observed for MPI from 20 to 25 processes. We further tested all four cases on a distributed architecture using MPI with 20, 25, 30, 35, and 40 processes. For all four cases, speedup plateaus using more than 25 processes. However, it is noted that the upper limit of the processes should be case and platform dependent for both OMP and MPI.

Additionally, MPI is generally faster than OMP for the same number of threads/processes (Fig. 7). This difference becomes smaller when the number of threads/processes is increased. As an exception, MPI (3.78 h) becomes slower than OMP (3.74 h) with 25 threads/processes. This can be explained by the fact that computation tasks are assigned to different threads implicitly by OMP while they are explicitly decomposed and distributed to different processes via MPI. However, the quick access to shared memory by different threads using OMP may be more advantageous than the message passing among different processes when a larger number of threads/processes are

used, which is why MPI becomes slower when the number of threads/processes is beyond a threshold such as 25 in Fig. 7.

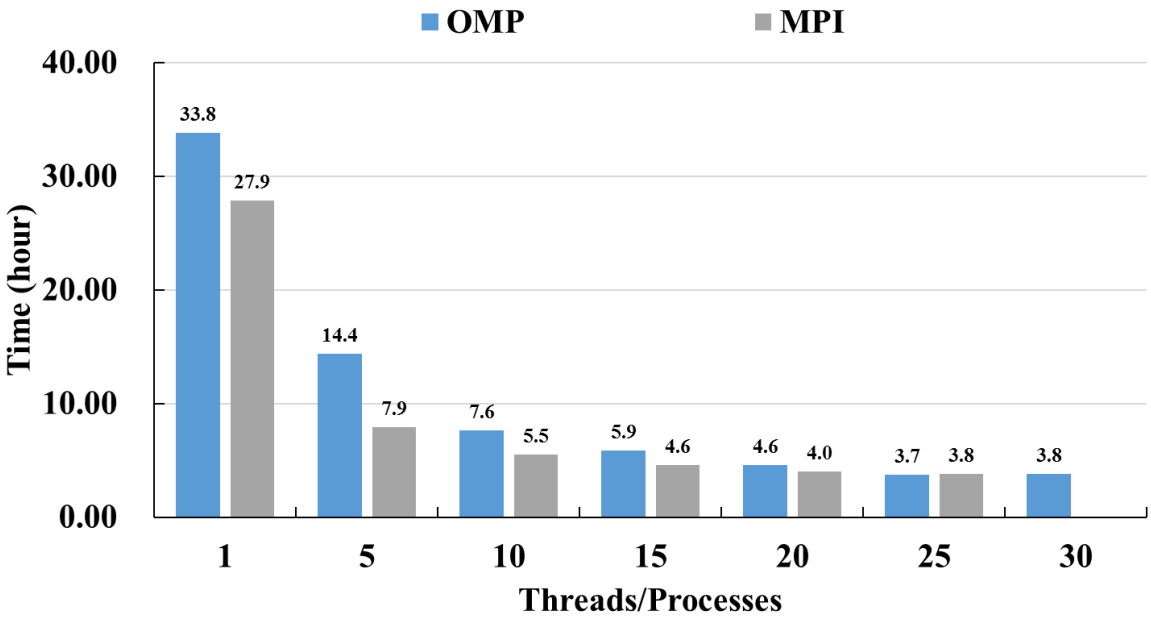

Fig. 7. Scaling tests for OpenMP- and MPI-version EcoSLIM using ER_Shrubs case.

4.2. Speedup by CUDA

Parallel performance for different APIs were plotted in Fig. 8. The original data and speedup were summarized in Tables 3 and 4. Results marked with OMP-*number* and MPI-*number* were obtained from the workstation where *number* represents number of threads/processes. Only those for 20 and 25 threads/processes are shown since no obvious speedup can be achieved when using more than 25 processes for all four cases. *GPU*-single represents results by using different GPU cards for the parallel with single-GPU described in section 2.3.3. OMP-*n*GPU represents results for multi-GPU with OpenMP using Tesla V100 cards where *n* is the number of GPU cards used. Ideal-*n*GPU represents results using multi-GPU which are scaled from the time of OMP-1GPU with the assumption of rigorous scaling.

For CUDA parallel using all three kinds of GPU cards, further speedup is observed over the upper limit of the CPU, i.e., MPI-25 here (Fig. 8b). Speedup relative to MPI-25 using single card is 1- ~ 2-fold for K80, 1- ~ 3-fold for 1080 Ti, and about 3-fold for V100 while that relative to OMP-1 is over 10-fold for all GPU cards with a maximum of 27.5 for V100 (Table 4). For OMP-4GPU, i.e., using 4 GPU cards with OpenMP, speedup achieves a maximum of 9.69-fold relative to MPI-25 and 87.82-fold relative to OMP-1 (Table 4). In addition, speedup by multi-GPU is higher with more particles. For example, it is 65.35-, 84.50-, 84.81-, and 87.82-fold speedup relative to OMP-1 for ER_Shrubs, ER_Trees, LW_Trees, and LW_Shrubs, with increasing particles number.

Difference between V100-Single and OMP-1GPU, also that between OMP-2GPU and Ideal-2GPU, and that between OMP-4GPU and Ideal-4GPU is the overhead of OpenMP (Fig. 8b and Table 3), which is minimal. Therefore, we can conclude that the current codes exhibit superior scaling performance with increasing GPUs for multi-GPU with OpenMP (Table 4 and Fig. 8b). It is also demonstrated better scaling if using more particles. For example, it is 3.69 and 2.01 (even beyond 2) for OMP-4GPU/OMP-1GPU and OMP-4GPU/OMP-2GPU for LW_Shrubs which has the maximum particles. Hence, for LW_Shrubs using 16 GPUs which is the maximum extension for multi-GPU with OpenMP (NVIDIA, 2019), the speedup is expected to be 351.82-fold (87.82×4) if converted from OMP-1. However, due to the scaling performance of MPI discussed in section 4.1, speedup could achieve 969-fold (9.69×25×4) if converted from MPI-25.

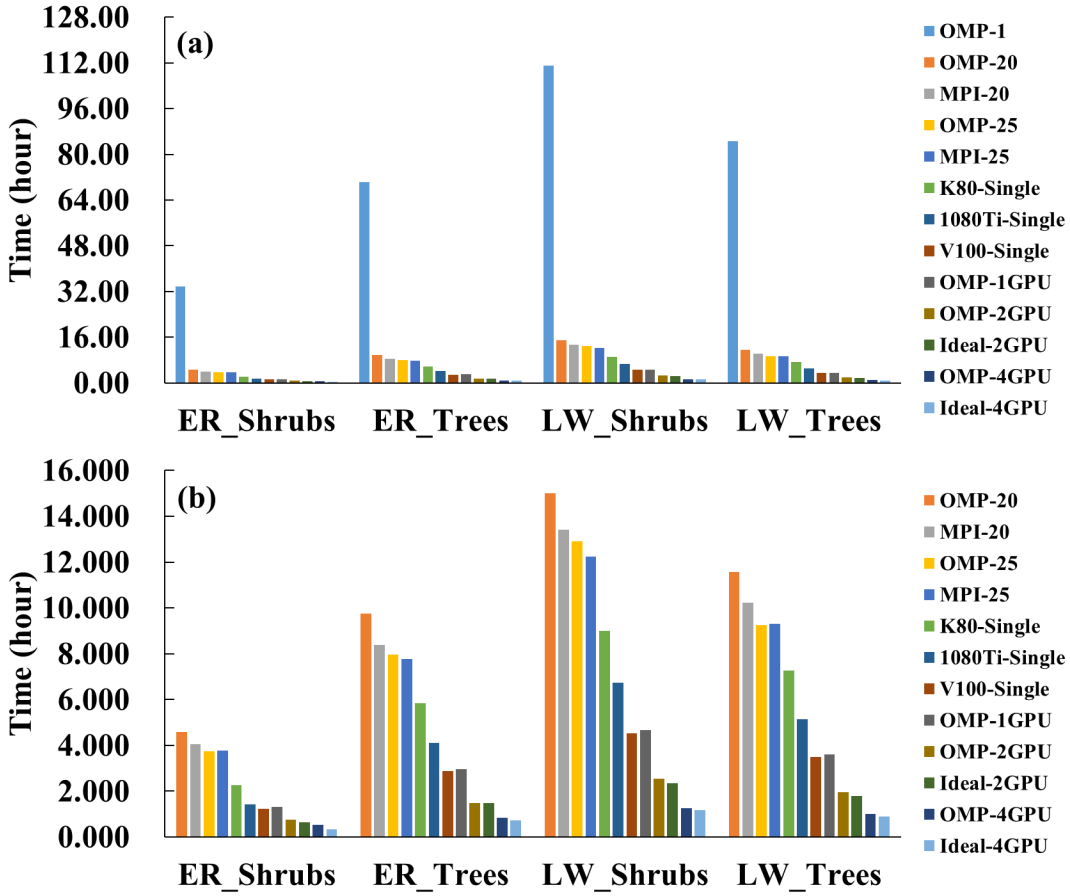

Fig. 8. Computation performance for different parallels. (b) is re-scaled from (a) without OMP-1.

Table 3. Time used by particle loop for different APIs (Unit: hour)

	ER_Shrubs	ER_Trees	LW_Shrubs	LW_Trees
OMP-1	33.8099	70.2118	111.0170	84.5417
OMP-20	4.5739	9.7658	15.0169	11.5777
OMP-25	3.7404	7.9578	12.9045	9.2516
MPI-20	4.0381	8.3705	13.4108	10.2140
MPI-25	3.7808	7.7594	12.2478	9.3124
K80-Single	2.2570	5.8318	8.9997	7.2757
1080Ti-Single	1.4119	4.0957	6.7310	5.1485
V100-Single	1.2310	2.8758	4.5249	3.4911
OMP-1GPU	1.3056	2.9561	4.6690	3.5950
OMP-2GPU	0.7546	1.4914	2.5448	1.9685
Ideal-2GPU	0.6528	1.4781	2.3345	1.7975
OMP-4GPU	0.5174	0.8309	1.2642	0.9968
Ideal-4GPU	0.3264	0.7390	1.1673	0.8988

389 **Table 4. Speedup for different parallel APIs (A/B: A relative to B)**

	ER_Shrubs	ER_Trees	LW_Shrubs	LW_Trees
K80-Single/OMP-1	14.9800	12.0395	12.3356	11.6197
1080Ti-Single/OMP-1	23.9464	17.1428	16.4934	16.4206
V100-Single/OMP-1	27.4654	24.4147	24.5347	24.2163
OMP-1GPU/OMP-1	25.8961	23.7515	23.7775	23.5165
OMP-2GPU/OMP-1	44.8051	47.0778	43.6250	42.9473
OMP-4GPU/OMP-1	65.3458	84.5009	87.8160	84.8131
K80-Single/MPI-25	1.6751	1.3305	1.3609	1.2799
1080Ti-Single/MPI-25	2.6778	1.8945	1.8196	1.8088
V100-Single/MPI-25	3.0713	2.6982	2.7068	2.6675
OMP-1GPU/MPI-25	2.8958	2.6249	2.6232	2.5904
OMP-2GPU/MPI-25	5.0103	5.2028	4.8129	4.7307
OMP-4GPU/MPI-25	7.3073	9.3385	9.6882	9.3423
OMP-2GPU/OMP-1GPU	1.7302	1.9821	1.8347	1.8263
OMP-4GPU/OMP-1GPU	2.5234	3.5577	3.6932	3.6065
OMP-4GPU/OMP-2GPU	1.4584	1.7949	2.0130	1.9748

390

391 ### 4.3. Toward large-scale simulations using multi-GPU

392 To test the capability of multi-GPU with OpenMP version of EcoSLIM at large scales, up to
393 2000 particles were added into the modeling domain per precipitation event. The maximum
394 permitted number of active particles is also increased from 3×10^7 to 3×10^8. Numerical experiment
395 was conducted based on ER_Shrubs with 4 Tesla V100. The maximum number of active particles
396 was achieved after about 2 years of simulation (Fig. 9a). The ratio of time used per timestep to the
397 number of active particles was plotted in Fig. 9b, which has a constant value of 0.023 in average.
398 We also tested that the maximum number of active particles on one V100 (16 GB) is about 2×10^8
399 due to the size of the memory. Hence, with the maximum extension of 16 V100 cards for OpenMP
400 (NVIDIA, 2019), the estimated computational time used for one-year simulation with hourly
401 resolution using 3.2 billion (0.2 billion×16) active particles would be only 44.77 hours. To our best
402 knowledge, this has been so far the largest application of Lagrangian particle tracking in subsurface
403 environment modeling, which shows a promising future of the EcoSLIM with multi-GPU.

For example, the particles number is 50,000 in Danesh-Yazdi *et al.* (2018), 80,000 in Jing *et al.* (2019), 100,000 in Jing *et al.* (2020), 765,000 in Kollet and Maxwell (2008b), 1 million in Engdahl and Maxwell (2015), and 4.14 million in Maxwell *et al.* (2016). In Wilusz *et al.* (2019) and Weill *et al.* (2019), which are the latest applications using IHM and particle tracking on RTDs, the number of particles injected into the modeling domain is 4,506,720 and 6.8 million in the whole simulation, respectively. More specifically, the number of active particles in this study (if using 16 V100 cards) is about 710-fold and 470-fold to those total injected in Wilusz *et al.* (2019) and Weill *et al.* (2019), respectively. If we count the total number of particles injected in the modeling domain, it is 1.11×10^{12} for the specific simulation in Fig. 9, which is evidently a huge step forward for improving the computational capability of EcoSLIM at exa-scales (e.g., continental).

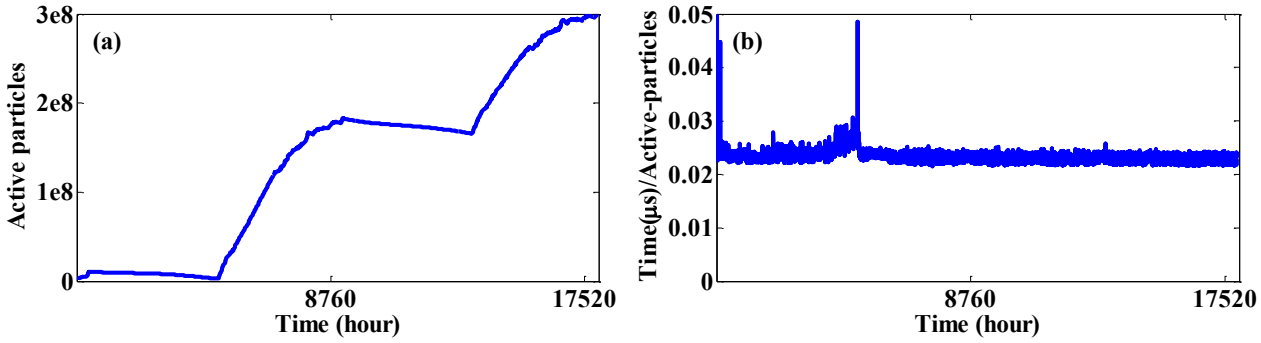

Fig. 9. Number of active particles (a) and the ratio of time used per timestep to number of active particles at that timestep. It is based on ER_Shrubs with 2000 particles added into the modeling domain per precipitation event and a maximum permitted number of active particles of 3×10^8. Test was conducted using 4 Tesla V100 with OpenMP.

5. Conclusions and perspectives

In this work, the EcoSLIM, a Lagrangian particle tracking program for calculating travel/residence time distributions (TTDs/RTDs), is accelerated via both MPI- and CUDA-parallelism. The latter is conducted through both single GPU and multi-GPU with OpenMP. The

MPI- and CUDA-parallel were verified by comparing the results to those from the original OpenMP parallel, which shows excellent agreement. The computation capability of EcoSLIM is drastically improved. With a maximum extension of 16 Tesla V100 cards and OpenMP, the wall clock time used for one-year simulation at hourly timesteps with 3.2 billion active particles is expected to be only 44.77 hours. The multi-GPU parallelism has demonstrated strong scalability especially using a very large number of particles. The accelerated EcoSLIM is expected to be a powerful tool for large-scale and long-term simulations with high spatiotemporal resolutions, which will advance our understanding of TTDs/RTDs under the evident climate change and intensified human disturbance. Although the current EcoSLIM is primarily developed to provide an efficient tool for simulating TTDs/RTDs, it can be extended to large scale contaminant transport modeling. In addition, the excellent performance of GPU parallel demonstrated in this study is expected to widely accelerate the next generation programs in subsurface environment modeling. Finally, it has to be noted that the tests based on ideal cases in this study are still limited. We expect more practical applications in the following work to further test and improve the computational capability of EcoSLIM.

Computer code availability

All codes for this work are publicly available on GitHub along with the Hillslope model used for the simulations: https://github.com/reedmaxwell/EcoSLIM

Acknowledgements

This study was supported by the National Natural Science Foundation of China (NSFC-41807198), by the Strategic Priority Research Program of Chinese Academy of Sciences (Grant No. XDA20100104), the Special Program for Applied Research on Super Computation of the NSFC-Guangdong Joint Fund (the second phase), by the U.S. Department of Energy Office of

447 Science, Offices of Advanced Scientific Computing Research and Biological and Environmental
448 Sciences IDEAS-Watersheds project, by the U.S. National Science Foundation
449 CyberInfrastructure project, HydroFrame (NSF-OAC 1835903), and by the U.S. National Science
450 Foundation INFEWS-China (NSF-1805160). This study was also supported by the Center for
451 Computational Science and Engineering of Southern University of Science and Technology and
452 the National Supercomputer Center in Guangzhou, China.
453

References

Basu, N.B., Jindal, P., Schilling, K.E., Wolter, C.F., Takle, E.S., 2012. Evaluation of analytical and numerical approaches for the estimation of groundwater travel time distribution. Journal of Hydrology 475, 65-73.

Benettin, P., Kirchner, J.W., Rinaldo, A., Botter, G., 2015. Modeling chloride transport using travel time distributions at Plynlimon, Wales. Water Resources Research 51, 3259-3276.

Benettin, P., Rinaldo, A., Botter, G., 2013a. Kinematics of age mixing in advection-dispersion models. Water Resources Research 49, 8539-8551.

Benettin, P., van der Velde, Y., van der Zee, S.E.A.T.M., Rinaldo, A., Botter, G., 2013b. Chloride circulation in a lowland catchment and the formulation of transport by travel time distributions. Water Resources Research 49, 4619-4632.

Botter, G., 2012. Catchment mixing processes and travel time distributions. Water Resources Research 48.

Botter, G., Bertuzzo, E., Rinaldo, A., 2011. Catchment residence and travel time distributions: The master equation. Geophysical Research Letters 38.

Cheng, W.L., Sheharyar, A., Sadr, R., Bouhali, O., 2015. Application of GPU processing for Brownian particle simulation. Computer Physics Communications 186, 39-47.

Danesh-Yazdi, M., Klaus, J., Condon, L.E., Maxwell, R.M., 2018. Bridging the gap between numerical solutions of travel time distributions and analytical storage selection functions. Hydrological Processes 32, 1063-1076.

de Rooij, R., Graham, W., Maxwell, R.M., 2013. A particle-tracking scheme for simulating pathlines in coupled surface-subsurface flows. Advances in Water Resources 52, 7-18.

476 DHI, 2019. MIKE Powered by DH GPU Guidelines, In: DHI (Ed.), Agern Allé 5 DK-2970
477 Hørsholm Denmark, p. 22.
478 Engdahl, N.B., Maxwell, R.M., 2015. Quantifying changes in age distributions and the hydrologic
479 balance of a high-mountain watershed from climate induced variations in recharge. Journal of
480 Hydrology 522, 152-162.
481 Engdahl, N.B., McCallum, J.L., Massoudieh, A., 2016. Transient age distributions in subsurface
482 hydrologic systems. Journal of Hydrology 543, 88-100.
483 Engdahl, N.B., Schmidt, M.J., Benson, D.A., 2019. Accelerating and Parallelizing Lagrangian
484 Simulations of Mixing-Limited Reactive Transport. Water Resources Research 55, 3556-3566.
485 Freedman, V.L., Bacon, D.H., Fang, Y., 2016. Integrated Disposal Facility FY 2016: ILAW
486 Verification and Validation of the eSTOMP Simulator, United States.
487 Hammond, G.E., Lichtner, P.C., Mills, R.T., 2014. Evaluating the performance of parallel
488 subsurface simulators: An illustrative example with PFLOTRAN. Water Resources Research
489 50, 208-228.
490 Hartmann, A., Jasechko, S., Gleeson, T., Wada, Y., Andreo, B., Barberá, J.A., Brielmann, H.,
491 Bouchaou, L., Charlier, J.-B., Darling, W.G., Filippini, M., Garvelmann, J., Goldscheider, N.,
492 Kralik, M., Kunstmann, H., Ladouche, B., Lange, J., Lucianetti, G., Martín, J.F., Mudarra, M.,
493 Sanchez, D., Stumpp, C., Zagana, E., Wagener, T., 2020. Danger of groundwater
494 contamination widely underestimated because of shortcuts for aquifer recharge,
495 https://eartharxiv.org/hdrje/, p. 17.
496 Jacobsen, D., Thibault, J., Senocak, I., 2010. An MPI-CUDA Implementation for Massively
497 Parallel Incompressible Flow Computations on Multi-GPU Clusters, 48th AIAA Aerospace
498 Sciences Meeting Including the New Horizons Forum and Aerospace Exposition.

Ji, X., Cheng, T., Wang, Q., 2010. A simulation of large-scale groundwater flow on CUDA-enabled GPUs, Proceedings of the 2010 ACM Symposium on Applied Computing. Association for Computing Machinery, Sierre, Switzerland, pp. 2402–2403.

Ji, X.H., Li, D.D., Cheng, T.P., Wang, X.S., Wang, Q., 2014. Parallelization of MODFLOW Using a GPU Library. Groundwater 52, 618-623.

Ji, X.H., Luo, M.L., Wang, X.S., 2019. Accelerating Streamline Tracking in Groundwater Flow Modeling on GPUs. Groundwater.

Jing, M., Heße, F., Kumar, R., Kolditz, O., Kalbacher, T., Attinger, S., 2019. Influence of input and parameter uncertainty on the prediction of catchment-scale groundwater travel time distributions. Hydrol. Earth Syst. Sci. 23, 171-190.

Jing, M., Kumar, R., Heße, F., Thober, S., Rakovec, O., Samaniego, L., Attinger, S., 2020. Assessing the response of groundwater quantity and travel time distribution to 1.5, 2, and 3 °C global warming in a mesoscale central German basin. Hydrol. Earth Syst. Sci. 24, 1511-1526.

Kirchner, J.W., Feng, X., Neal, C., 2001. Catchment-scale advection and dispersion as a mechanism for fractal scaling in stream tracer concentrations. Journal of Hydrology 254, 82-101.

Kirchner, J.W., Feng, X.H., Neal, C., 2000. Fractal stream chemistry and its implications for contaminant transport in catchments. Nature 403, 524-527.

Kollet, S.J., Maxwell, R.M., 2008a. Capturing the influence of groundwater dynamics on land surface processes using an integrated, distributed watershed model. Water Resources Research 44.

Kollet, S.J., Maxwell, R.M., 2008b. Demonstrating fractal scaling of baseflow residence time distributions using a fully-coupled groundwater and land surface model. Geophysical Research Letters 35.

Kuffour, B.N.O., Engdahl, N.B., Woodward, C.S., Condon, L.E., Kollet, S., Maxwell, R.M., 2020. Simulating coupled surface–subsurface flows with ParFlow v3.5.0: capabilities, applications, and ongoing development of an open-source, massively parallel, integrated hydrologic model. Geosci. Model Dev. 13, 1373-1397.

LaBolle, E.M., Fogg, G.E., Tompson, A.F.B., 1996. Random-Walk Simulation of Transport in Heterogeneous Porous Media: Local Mass-Conservation Problem and Implementation Methods. Water Resources Research 32, 583-593.

Małoszewski, P., Zuber, A., 1982. Determining the turnover time of groundwater systems with the aid of environmental tracers: 1. Models and their applicability. Journal of Hydrology 57, 207-231.

Manning, A.H., Clark, J.F., Diaz, S.H., Rademacher, L.K., Earman, S., Niel Plummer, L., 2012. Evolution of groundwater age in a mountain watershed over a period of thirteen years. Journal of Hydrology 460-461, 13-28.

Maxwell, R.M., Condon, L.E., Danesh-Yazdi, M., Bearup, L.A., 2019. Exploring source water mixing and transient residence time distributions of outflow and evapotranspiration with an integrated hydrologic model and Lagrangian particle tracking approach. Ecohydrology 12.

Maxwell, R.M., Condon, L.E., Kollet, S.J., Maher, K., Haggerty, R., Forrester, M.M., 2016. The imprint of climate and geology on the residence times of groundwater. Geophysical Research Letters 43, 701-708.

Maxwell, R.M., Miller, N.L., 2005. Development of a coupled land surface and groundwater model. Journal of Hydrometeorology 6, 233-247.

McDonnell, J.J., McGuire, K., Aggarwal, P., Beven, K.J., Biondi, D., Destouni, G., Dunn, S., James, A., Kirchner, J., Kraft, P., Lyon, S., Maloszewski, P., Newman, B., Pfister, L., Rinaldo,

A., Rodhe, A., Sayama, T., Seibert, J., Solomon, K., Soulsby, C., Stewart, M., Tetzlaff, D., Tobin, C., Troch, P., Weiler, M., Western, A., Wörman, A., Wrede, S., 2010. How old is streamwater? Open questions in catchment transit time conceptualization, modelling and analysis. Hydrological Processes 24, 1745-1754.

Molinero, D., Galván, S., Pacheco, J., Herrera, N., 2019. Multi GPU Implementation to Accelerate the CFD Simulation of a 3D Turbo-Machinery Benchmark Using the RapidCFD Library. Springer International Publishing, Cham, pp. 173-187.

NVIDIA, 2019. NVIDIA DGX-2 The world's most powerful deep learning system for the most complex AI challenges. NVIDIA, p. 2.

Porter, A.R., Appleyard, J., Ashworth, M., Ford, R.W., Holt, J., Liu, H., Riley, G.D., 2018. Portable multi- and many-core performance for finite-difference or finite-element codes – application to the free-surface component of NEMO (NEMOLite2D 1.0). Geosci. Model Dev. 11, 3447-3464.

Ruetsch, G., Fatica, M., 2014. CUDA Fortran for scientists and engineers : best practices for efficient CUDA Fortran programming. Morgan Kaufmann, an imprint of Elsevier, Amsterdam Boston.

Scheibe, T.D., Smith, J.C., 2015. Multiscale Computation: Needs and Opportunities for BER Science, United States.

Steefel, C.I., Appelo, C.A.J., Arora, B., Jacques, D., Kalbacher, T., Kolditz, O., Lagneau, V., Lichtner, P.C., Mayer, K.U., Meeussen, J.C.L., Molins, S., Moulton, D., Shao, H., Šimůnek, J., Spycher, N., Yabusaki, S.B., Yeh, G.T., 2015. Reactive transport codes for subsurface environmental simulation. Computational Geosciences 19, 445-478.

Su, D., Ulrich Mayer, K., MacQuarrie, K.T.B., 2017. Parallelization of MIN3P-THCm: A high performance computational framework for subsurface flow and reactive transport simulation. Environmental Modelling & Software 95, 271-289.

Sun, H., Ji, X., Wang, X.-S., 2019. Parallelization of groundwater flow simulation on multiple GPUs, Proceedings of the 3rd International Conference on High Performance Compilation, Computing and Communications. Association for Computing Machinery, Xi'an, China, pp. 50-54.

Tompson, A.F.B., 1993. Numerical simulation of chemical migration in physically and chemically heterogeneous porous media. Water Resources Research 29, 3709-3726.

Tompson, A.F.B., Gelhar, L.W., 1990. Numerical simulation of solute transport in three-dimensional, randomly heterogeneous porous media. Water Resources Research 26, 2541-2562.

van der Velde, Y., de Rooij, G.H., Rozemeijer, J.C., van Geer, F.C., Broers, H.P., 2010. Nitrate response of a lowland catchment: On the relation between stream concentration and travel time distribution dynamics. Water Resources Research 46.

Weill, S., Lesparre, N., Jeannot, B., Delay, F., 2019. Variability of Water Transit Time Distributions at the Strengbach Catchment (Vosges Mountains, France) Inferred Through Integrated Hydrological Modeling and Particle Tracking Algorithms. Water 11, 2637.

Wilusz, D.C., Harman, C.J., Ball, W.B., Maxwell, R.M., Buda, A.R., 2019. Using particle tracking to understand flow paths, age distributions, and the paradoxical origins of the inverse storage effect in an experimental catchment. Water Resources Research n/a, e24397.

Xu, S., Huang, X., Oey, L.Y., Xu, F., Fu, H., Zhang, Y., Yang, G., 2015. POM.gpu-v1.0: a GPU-based Princeton Ocean Model. Geoscientific Model Development 8, 2815-2827.

Yang, J., Heidbüchel, I., Musolff, A., Reinstorf, F., Fleckenstein, J.H., 2018. Exploring the Dynamics of Transit Times and Subsurface Mixing in a Small Agricultural Catchment. Water Resources Research 54, 2317-2335.